

COMPONENT PART NOTICE

THIS PAPER IS A COMPONENT PART OF THE FOLLOWING COMPILATION REPORT:

TITLE: Transonic and Supersonic Phenomena in Turbomachines: Proceedings of the Propulsion and Energetics (68th)(B) Specialists' Meeting Held in Munich, Germany on 10-12 September 1986.

TO ORDER THE COMPLETE COMPILATION REPORT, USE AD-A182 996

THE COMPONENT PART IS PROVIDED HERE TO ALLOW USERS ACCESS TO INDIVIDUALLY AUTHORED SECTIONS OF PROCEEDING, ANNALS, SYMPOSIA, ETC. HOWEVER, THE COMPONENT SHOULD BE CONSIDERED WITHIN THE CONTEXT OF THE OVERALL COMPILATION REPORT AND NOT AS A STAND-ALONE TECHNICAL REPORT.

THE FOLLOWING COMPONENT PART NUMBERS COMPRISE THE COMPILATION REPORT:

AD#: AD-P005 506 thru AD-P005 523. AL#: _____
AD#: _____ AD#: _____
AD#: _____ AD#: _____

Accession For	
NTIS GRA&I	<input checked="" type="checkbox"/>
DTIC TAB	<input type="checkbox"/>
Unannounced	<input type="checkbox"/>
Justification	
By _____	
Distribution/	
Availability Codes	
Dist	Avail and/or Special
A-1	

DTIC
SELECTE
S AUG 17 1987 D
A

DTIC FORM 463
MAR 85

This document has been approved for public release and sale; its distribution is unlimited.

OPI: DTIC-TID

DOWNSTREAM FLOW ANGLE CORRELATIONS FOR TURBINE CASCADES IN
SUBSONIC AND TRANSONIC FLOW CONDITIONS

by

W. Rieß
P. Dalbert
Institut für Strömungsmaschinen
Universität Hannover

Appelstr. 9
D-3000 Hannover
Germany

P.-A. Gieß
H.-J. Heinemann
Inst. für Exp. Strömungsmechanik
Deutsche Forschungs- und Versuchsanstalt
für Luft- und Raumfahrt
Bunsenstr. 10
D-3400 Göttingen
Germany

SUMMARY

Extensive experimental and theoretical investigations of different turbine cascades have been performed within the transonic Mach number range. Some problems related to measurements in rectilinear cascades are discussed. From the done flow field calculations using a 2-d time-marching Euler code limitations can be determined when applying the computer code itself as well as when comparing the calculated data with experimental ones. Experimental and theoretical results within the subsonic Mach number range are used to check the accuracy of "simplified methods" for calculating the downstream flow angle.

1. INTRODUCTION

The great variety of possible and applicable turbine blade profile forms has precluded so far the accumulation of systematic and rather exhaustive aerodynamic data, as are available for axial compressor blades - at least in the subsonic regime. Therefore, as well as for the development and optimisation of new profile forms as for the detailed calculation of multi-stage turbine bladings, methods are necessary for the sufficiently exact calculation of

- outlet angle
 - aerodynamic loss coefficient
- in the whole subsonic-compressible and - mainly for gas turbines - in the transonic flow regime in the great numbers of cases, where pertinent experimental data are not available.

Loss calculation has made progress by combined application of modern cascade flow and boundary layer methods. Outlet angle calculation by flow field methods still comprises some uncertainties, mainly connected with the formulation of the trailing edge condition, and the practical application seemingly encounters often some doubt. Furthermore it necessitates a not negligible effort in the preparation and the execution of computer calculations and, consequently, the turbo machine industry still prefers to apply widely different "simplified methods" - e.g. the well known Sine Law for the calculation of outlet angle. All of these are based on balances of mass flow and momentum in the outlet region of the cascade and necessitate various simplifying assumptions.

Because of the differing experiences in application of "simplified methods" and, to some extent, of modern cascade flow calculation methods, a research project was initiated by Forschungsvereinigung Verbrennungskraftmaschinen (FVV) and carried out jointly by Institut für Strömungsmaschinen (IfS), Universität Hannover, and Institut für Experimentelle Strömungsmechanik (SM-ES) at Deutsche Forschungs- und Versuchsanstalt für Luft- und Raumfahrt (DFVLR), Göttingen. It comprises:

- experimental investigation of downstream flow angle, loss coefficient and pressure distribution for several cascades in the transonic regime (DFVLR, chapter 2),

- flow field calculation using a transonic time marching procedure and comparison with experimental data (DFVLR, chapter 3),
- experimental investigation of downstream flow angle, loss coefficient and pressure distribution for several cascades in the subsonic-compressible regime (IfS, chapter 4),
- flow field calculations using a subsonic-compressible finite difference method and comparison with experimental data (IfS, chapter 5),
- comparison of downstream flow angle data from several "simplified methods" with experimental results for more than thirty different turbine cascades (IfS, chapter 6).

The project resulted in a deeper insight in the potential and the limitations of the different methods and a better understanding of the aerodynamic characteristics of turbine cascades.

2. EXPERIMENTAL INVESTIGATIONS ON TRANSONIC TURBINE CASCADES

At DFVLR the experimental task within the scope of this project has been to re-measure three different profiles in one cascade geometry each and a fourth profile in six different cascade geometries. All these cascades have been investigated for the design incidence flow angle and within the downstream Mach number range $0.2 < Ma < 1.3$. From the obtained wake traverses, surface pressure distributions and Schlieren photographs documented in [6] a few examples are taken to discuss some typical problems of transonic turbine cascade flow.

2.1 Test facility

A detailed description of the test-facility for rectilinear cascades (EGG) of DFVLR, Göttingen is given in [1]. The cascade assembly drawn to scale is shown in *FIGURE 1* for a hub-section cascade. The width of the flow channel which is equal to the height of the cascade blades is 125 mm. In general, the profile chord length is 60 mm and therefore the aspect ratio is 2.08. There are approximately 8 blades in the flow field in the case of stator cascades and up to 15 in the case of rotor cascades.

Some blades of the cascade are fixed into glass panes to allow the Schlieren pictures to be taken. For surface pressure distribution measurements, one of the blades is substituted by an instrumented one. For this subject the panes of glass in the cascade rig are replaced by steel plates.

2.2 Upstream flow

In the upstream flow field total pressure, total temperature, and humidity of the air are measured in the settling chamber. The upper and lower walls of the rectangular nozzle can be adjusted in horizontal and vertical direction and can be set to angles up to $\pm 4^\circ$ relative to the centre line. These adjustments are used to set the inlet flow conditions to periodicity as well as possible. The wall static pressure can be measured in a plane parallel to the cascade inlet front at 96 positions distributed over all blade passages on one instrumented side-wall. Values from 47 ports are acquired, D1 to D47 in fig. 1.

Through holes on the opposite side wall in the very same plane, the incidence angle can be measured with a wedge probe at 7 different locations, W1 to W7. The check of this angle is necessary because experience has shown that the actual incidence angle can differ by up to $\pm 2^\circ$ from the geometric one. The incidence angle distribution as well as the static pressure distribution show a remarkable dependence on the position of the upper and lower walls.

With the adjustable walls variations in the flow angle can be kept within the range of some tenth of a degree. In *FIGURE 2* the distribution of the inlet Mach number based on static pressures, D8 to D42, and total pressure in the settling chamber

shows that, for two flow conditions, the distribution is quite uniform except for the region close to the upper and lower walls.

FIGURE 3 shows the dependence of inlet Mach number on outlet Mach number. The choking Mach number is about 0.5 corresponding to a downstream Mach number of about 0.9. For higher flow accelerations no changes in the upstream flow occur.

Tests lead to higher inlet Mach numbers than can be expected for 2-d flow [2]. This is due to the relatively long inlet duct which causes a turbulent boundary layer of about 30 mm thickness on both sides. In the future an adaptive nozzle will be used which is shorter in order to approximate 2-d flow conditions better.

2.3 Downstream flow

Usually, downstream of the cascade, the flow is not guided by walls and therefore free shear layers originate from both the top and bottom blades. The interference of obstacles crossing the whole channel in the downstream supersonic flow field is demonstrated by Schlieren pictures (flash duration: 50 nsec) in *FIGURE 4*. Four pitches downstream cylinders of different diameters are inserted. Severe distortions of the flow are evident even if the diameter of the cylinder is only about twice of the blade's trailing edge thickness. This was taken into account by designing the probe with a long axial stem and mounting the probe support as far downstream as possible, [3]. In *FIGURE 5* Schlieren pictures show the probe head within the flow.

A wedge-type probe, [3], specially designed for tests in the complex supersonic cascade flow fields is traversed at a fixed angle. From the probe's readings the local values for total and static pressure and flow angle are evaluated within the calibration range for the flow angle of $\pm 6^\circ$.

In *FIGURES 6 and 7* sample measured distributions of local flow angle, total pressure and Mach number are shown for a stator cascade. In the case of subsonic flow results are shown for about 7 different pitches beginning from the free shear layer at the bottom. About 2 pitches from this boundary the wakes are almost identical. The rig consists of two more blades. For those blades measurements could not be provided due to the restrictions of the support system. This would be possible with the system in use today because the downstream area is now covered with 800 mm instead of the previous 314 mm.

In the supersonic case the flow is often less periodic. The expansion around the trailing edges can lead to a smaller flow angle at the bottom blade and to a higher one at the top blade. This may cause an angle gradient in the flow field.

Trailing edge shocks are reflected from the free shear layer and its influence on the flow pattern can be considerable, especially when causing additional shock boundary layer interactions or flow separation at the blades. For the example given in the figure the results for the 3 pitches of the centre blades show a quite periodic outlet flow field, which may not be achieved in all cases.

Additional reasons for deviations of the flow behind different pitches are due to the unavoidable imperfections of the hardware. Formerly blades were manufactured by copy-machining from a template. For some years the blades have been wire-eroded from brass which is a more precise method. The actual shape of the instrumented blade is measured with a ZEISS UMM 500 and is compared with the desired contour. Usually, deviations normal to the surface are within 5/100 mm. These maximum deviations occur at the leading edge and trailing edge, respectively. They are primarily due to the technology used to instrument the blade, [1]. An important geometric quantity is the throat, c^* , i.e. the shortest distance between two adjacent blades, fig. 1; numbers differ up to 3/10 mm. For calculating the 1-d theoretical choking Mach number, an averaged value of c^* is used.

From the data of the inhomogeneous flow in the traverse plane, the properties of an equivalent uniform downstream flow are obtained by applying the equations of conservation of mass, momentum and energy [4]. Results of data for downstream flow angle, total pressure loss, and axial velocity density ratio as functions

of downstream Mach number are given in *FIGURES 8 to 10* for the cascade shown in *fig. 1*.

2.4 Pressure distribution

In *FIGURE 11* a measured surface pressure distribution is shown. The pressure coefficient

$$(1) \quad c_{p1}^* = [p_k^* - p_1^*] / p_1^* \quad \text{and} \quad p_1^*/p_{01}^* = [2/(\kappa+1)]^{\kappa/(\kappa-1)}$$

is plotted versus the axial length of the cascade, XA/LA . In *FIGURE 12* the pressure distribution cp_1^* is plotted versus YA/LU , the coordinate perpendicular to the axial direction, and combined with the corresponding Schlieren picture which allows an easy comparison.

Exemplarily, the suction side flow behaviour is discussed: the flow is accelerated from the stagnation point at $YA/LU = 0.4$ continuously up to $YA/LU = 0.0$. An area of recompression/expansion follows up to $YA/LU = 0.3$. From there the flow is accelerated up to $YA/LU = 0.7$ where the trailing edge shock from the adjacent blade is reflected which causes a shock boundary layer interaction. Further downstream the flow is decelerated and finally forms a shock at the trailing edge.

By integrating pressure distributions aerodynamic forces on the blades can be determined. These values can be cross-checked with those evaluated from data reduction of the wake flow measurements. In *FIGURE 13* results are shown for the normal force coefficient, normal to the chord direction, and for the tangential force coefficient. Only the results for the first seem to agree quite well. The deviations are related to the fact that friction forces are taken into account by probe measurements but not by static pressure measurements on the blades.

3. THEORETICAL INVESTIGATIONS OF TRANSONIC TUFFINE CASCADES

At DFVLR the theoretical task of the project has been to perform flow field calculations applying a 2-d time-marching Euler code for seven different cascades for subsonic and transonic downstream Mach numbers. These data have been used to determine limitations of the application of the computer code itself as well as to check some assumptions which are necessary for "simplified methods" to calculate the angle of the homogeneous downstream flow. Some typical results are discussed and compared with experiments.

3.1 Computer code

A finite volume method, [2], is used to solve the time-dependent Euler equations for 2-d compressible flow. The boundary conditions prescribed in the computer code are total pressure, total temperature and direction of the homogeneous flow upstream of the cascade and the static pressure downstream. The spatial discretisation is based on a H-grid which is systematically refined in four steps. Refinement is done by doubling the number of quasistreamlines as well as the number of nodes on a quasistreamline. In *FIGURE 14* a second mesh consisting of relatively widely spaced grid points is shown. From the final solution of the coarser grid initial values for the next finer one are interpolated. The values of the homogeneous flow are calculated using the conservation laws according to [4] after each time interval.

Formerly the vanishing local pressure change on the blade contour was used to define a criterion for the "steady state" solution with iteration in time. For this project the "steady state" was based on the vanishing changes of the homogeneous downstream flow quantities, [5]. These time-dependent values approach the "steady state" with variations of decreasing amplitude. In *FIGURE 15* the "steady state" values for the four grids after 40, 80, 160 and 320 time intervals are shown for downstream flow angle, pressure loss coefficient, upstream and downstream Mach number and the axial velocity density ratio. Allowing deviations from this "steady

state" value of about $\Delta\beta \pm 1.0^\circ$, $\pm 0.5^\circ$, $\pm 0.25^\circ$ or $\pm 0.1^\circ$, in the four meshes respectively, as the maximum amplitudes for the downstream flow angle then the "steady state" is approximated sufficiently after 10, 20, 40 and 80 time intervals. The accuracy achieved for the other flow quantities is given in the figure, too. There is a significant change of the steady state values in the first three meshes, while in the finest mesh only local values vary, especially near the leading and trailing edge, [5]. If one takes into account that the experimental error in general corresponds to the accuracy prescribed in the third mesh, the accuracy of the final solution is sufficient.

3.2 Application of the computer code

• Surface pressure distribution

In *FIGURE 16* the surface pressure distribution for a low subsonic downstream Mach number in cascade 10.1.2 with the designed blades is shown. The comparison of experimental and calculated data indicates some significant deviations marked by arrows. Another calculation using Katsanis' code, [6], results in a very similar pressure distribution with irregularities at the same locations. In the case of transonic downstream Mach number in fig. 11 the corresponding deviations are to be seen.

The two main reasons which cause these deviations are first the inaccuracies of the manufactured blades forming the cascade 10.1.2I and second 3-d effects because of the side-wall boundary layers resulting in an axial velocity density ratio μ not equal to 1.0. The irregularities of the surface pressure distribution vanish when the actual cascade 10.1.2I is computed, fig. 11 and 16. The remaining difference to the experimental values can be reduced again by introducing the axial velocity density ratio from the measurements given in fig. 10 to the code. This leads to a remarkable agreement of experimental and calculated data for both subsonic as well as for transonic downstream Mach number.

The calculated blade force coefficients determined from homogeneous flow quantities on one hand and from pressure distributions on the other give nearly the same results, fig. 13. In spite of the abovementioned deviations in the pressure distribution, after integration the calculated results for cascade 10.1.2 and experimental ones for cascade 10.1.2I agree quite well.

• Influence of blade variations

The blades used in the basic cascade 10.1.2 have very thin trailing edges, i.e. low values of d/t see *TABLE 1*, and a curved suction side downstream of the throat. The variation of the flow field due to changes of the blade's suction side and trailing edge have been investigated in cascades 10.SSV1 and 10.SSV2. The blade shapes in *FIGURE 17* indicate the increase of the trailing edge diameter, the reduction of the curvature of the suction side and identical contours up to the throat. Therefore the geometry of the cascade variations has been chosen to give the same flow channel up to the throat as in cascade 10.1.2. Due to the different chord length of the blades the pitch chord ratios in tab. 1 are slightly different.

In fig. 17 the calculated pressure distributions for a downstream Mach number of $Ma_{2is} = 0.670$ are shown. There is an increase of the velocity level on the blade surface related to the increase of the trailing edge thickness. The difference between the pressure distributions for the two cascade versions is less than that between the basic one and version 10.SSV2. Due to the unchoked flow condition the whole flow field is influenced by the thick trailing edge. The stronger expansion around the thicker trailing edges causes the increasing differences between the local pressure maximum and minimum. Based on this expansion there is an upstream shift of the crossing of the pressure curves of the suction and the pressure side. In *FIGURE 18* the experimental results for other flow conditions indicate the same behaviour. In the case of transonic downstream Mach number, i.e. for a choked cascade, there are identical pressure distributions up to the throat, *FIGURE 19*. Moreover the pressure distributions indicate an increasing strength of the shock reflected on the suction side with increasing trailing edge thickness.

In the throat, constant flow velocity and constant flow direction perpendicular to the throat, are assumed when using "simplified methods" to calculate the angle

of the homogeneous downstream flow. For cascade 10.SSV2 the local flow direction in the throat calculated by the time marching procedure (TMP) indicates significant deviations from this assumption, see *FIGURE 20*. This may be related to the thick trailing edge but in cascade 3.1.1, having blades with thin trailing edges, there are remarkable differences, too. In addition the local flow velocity varies by about $\pm 10\%$ from an averaged value, [5]. As the abovementioned assumptions are not proven by the time-marching procedure in these cases significant differences between the downstream flow angle calculated using one of the "simplified methods" and experimental results may be expected.

3.3 Homogeneous flow quantities

• Upstream flow

For cascade 10.1.2 the homogeneous upstream flow indicates that the experimental upstream Mach number is higher than the corresponding calculated one, fig. 3, due to side-wall boundary layers in the wind tunnel. Correcting the geometric cross-section with the displacement thickness a corrected experimental inlet Mach number for 2-d flow can be calculated. The results from the flow field calculation for cascade 10.1.2 and 10.1.2I using $\mu = 1.00$ fit this curve quite well. On the other hand it is possible to take into account different cross-sections in calculation planes 1 and ME and linear interpolation in-between and to perform a quasi-3-d calculation corresponding to the experimental value μ not equal to 1.00. The result for cascade 10.1.2I is an upstream Mach number close to that of the experiment.

Due to the thick trailing edges of the blades in cascades 10.SSV1 and 10.SSV2 the mass flow changes for subsonic downstream Mach number $Ma_{2is} \approx 0.67$. There is a significant difference for the basic cascade and the variations, while the two variations have nearly the same upstream Mach number. The expansion around the thicker trailing edges results in a higher level of the contour velocities and therefore more mass flows through the cascade. To increase the mass flow in cascade 10.1.2 to that value the isentropic downstream Mach number has to be increased to $Ma_{2is} = 0.70$.

• Downstream flow

From the local flow quantities in calculation plane ME the values of the homogeneous downstream flow are computed. For the basic cascade 10.1.2 the downstream flow angle in fig. 8 from experiment and calculation fit to the same curve. This is related to the fact that the values of the pressure loss coefficients, ζ (ZETA), in fig. 9 are close to each other, i.e. for the subsonic case numerical losses due to smoothing the solution and for the transonic case numerical losses and predicted shock losses are comparable to the measured ones. All this is related to the thin trailing edge of the blades.

For the cascades having blades with thicker trailing edges the downstream flow angle in fig. 8 increases. This can be seen in the case of the blade variations as well as in the case of the actual blade. The corresponding pressure loss coefficients in fig. 9 increase as well. When smoothing the expansion around a thick trailing edge obviously from the subsonic case the numerical viscosity increases. This gives a hint for the necessity of a wake model to be incorporated in the procedure especially for thick trailing edges.

For the axial velocity density ratio, μ (MY), in fig. 10 it can be seen that the calculated values are close to 1.00, while the experimental ones are significantly different. As mentioned above this is because of the higher upstream Mach number due to side-wall boundary layers. If these geometric modifications of the flow channel are introduced to the code the calculated values are close to the experimental ones.

4. EXPERIMENTAL INVESTIGATIONS ON SUBSONIC TURBINE CASCADES

Parallel to the transonic cascade investigations described above measurements and calculations in the subsonic-compressible range were conducted at IfS, Hannover.

For two different profiles geometrical modifications of the outlet part of the suction side combined with an increase of the trailing edge thickness were investigated in a range of downstream Mach number of 0.2 to about 0.8. Wake traverses and surface pressure measurements were made and in addition some L-2-F velocity measurements in the throat area for comparison with flow field calculations. A few results are presented here.

4.1 Test Facility

The cascade tunnel used is of the suction type. It is shown in *FIGURE 21*. The blades of 240 mm length are mounted between two circular side wall plates which can be rotated so that the outlet flow is directed roughly vertically downwards. One of the side plates is made of steel and comprises the probe insert and traversing provisions, furthermore the outlets for the static pressure taps on the blades. The other side plate has a glass insert and allows measurements with a L-2-F anemometer between the blades and behind the cascade. With a blade chord length between 80 and 100 mm the aspect ratio realized is 2.4 to 3. Because of the limited airflow capacity available a rather limited number of six to eight blades constituted the cascade.

The flow channel consists of two fixed, sector-shaped side walls and two adjustable guide plates which are set at the intended angle. The quality of the inlet flow is controlled by static pressure taps all along the guide plates and in front of the cascade. The uniformity of the inlet flow is remarkably good. The side wall boundary layers are according to our measurements thin.

Since the outlet plenum is not sufficiently large for an undisturbed free jet outlet, the flow behind the cascade is protected against uncontrollable influences from the direct environment by adjustable guide plates. This, however poses the problem to avoid influencing the flow, especially the outlet angle. This problem was - in most cases sufficiently to satisfaction - solved by using pressure taps on the guide plates and behind the cascade for adjusting the guide plates to a nearly uniform pressure distribution. Nevertheless this configuration of cascade tunnel will always pose operational problems. A further operational limitation results from the expansion of the more or less moist air in the cascade which leads to spontaneous condensation under transonic flow conditions and a falsification of the results. The outlet Mach number has to be limited to about 0.8.

4.2 Downstream Flow

For the determination of the outlet flow a wedge-type five-hole probe (*FIGURE 22*) was used. The long axial stem built according to DFVLR experiences minimizes the interference of the holder with the flow. The probe is traversed at a fixed angle. The flow direction is calculated from the calibration factors. Because of the geometrical limitations at the tunnel the traversing travel was only about two pitches lengths which is not enough to smooth out statistical scattering. In the subsonic region, however, the results were quite satisfactory.

Measurements were made - among others - for the cascade configurations described above (fig. 5 and 17 resp.). *FIGURE 23* shows local distributions of the flow angle, total and static pressure and Mach number. The decrease of uniformity and periodicity with increasing trailing edge thickness is obvious. The comparison of the parameters flow angle $BETA_2$, loss factor XI and inlet Laval number LA_1 - all calculated from the test data also according to [4] - with the same data from the DFVLR measurements is shown in *FIGURE 24*. The differences, keeping in mind some unavoidable shortcomings of the IfS measurements, are rather small and the general compatibility is good. Similarly good agreement has been found for the blade pressure distributions which is not shown here in detail.

5. THEORETICAL INVESTIGATIONS OF SUBSONIC TURBINE CASCADES

5.1 Computer Code

For the calculation of subsonic-compressible flow fields in turbine cascades a finite difference method for calculation of the stream function acc. to Katsanis, [6], was used after some adaptations to our problem. The solution yields the 2-d subsonic-compressible, frictionless flow field for a given geometry and given inflow and outflow conditions. Contour Mach numbers up to 0.7 could well be handled.

5.2 Application of the computer code

It is well known that methods like this demand an additional information defining the total circulation around the profiles to render a correct solution, i.e. the outlet angle should be available as input which poses some problems in all cases where experimental data are not already available. Test calculations for a number of different cascades with prescription of three or four slightly differing outlet angle values showed, that - provided the calculating net and the contour point spacing are fine enough at the trailing edge - the "correct" outlet angle value can quite easily be deduced by visual inspection of the pressure distribution diagrams with some experience. A "normal" closure of the pressure curve at the trailing edge is a good indicator. It seems highly probable that the introduction of an extra iteration level in the code which satisfies p.e. identical velocity (or static pressure) at the both end points of the halfcircle of a non-zero thickness trailing edge, will allow the direct calculation of a flow field with an outlet angle correct to a few tenths of a degree (see fig 16). Experience showed, as mentioned already for the time marching method, that high accuracy for the geometrical input data is indispensable for a quality solution. Small differences cause considerable disturbances in the solution (fig. 16).

Very important, too, for the comparison of measured and calculated contour pressure distribution curves is the introduction of the experimental value of the axial velocity density ratio into the calculation, if it deviates - as often - sensibly from unity. *FIGURE 25* shows results with and without correction.

6. DOWNSTREAM FLOW ANGLE CORRELATION

6.1 "Simplified Methods" for Outlet Flow Angle Calculation

Almost since the beginning of turbomachine theory the need for methods for the theoretical prediction of the outlet flow angle covering a large variety of profile forms and a great range of operating conditions was felt. In course of time a host of - in principle - quite generally applicable methods was developed, beginning with the famous Sine Law, described p.e. in a modern form in [8]. Further exist the Tangent Law, [9], and its more generalized form in [14], the methods of Fricke, [10], and Oedegard, [11], which take into account the compressibility of the fluid and finally, also classical example, the Jet Deflection Law, [12], for transonic conditions only.

The practical experiences with all these methods were differing widely. The deviations from experimental data seemed somewhat erratic and unpredictable. The research project the results of which are reported here very partially, was started originally in order to check the results and the accuracy of all these "simplified methods" for the calculation of outlet flow angle in a wide range of profile form and operating conditions against proven experimental results of high quality and thus decide their practical applicability. Experimental data were collected or produced for about 60 cascade configurations with more than 30 different profile forms. *FIGURE 26* gives a synoptical presentation of the cascade characteristics in an inflow - outflow angle manner. *FIGURE 27* shows the range of outlet flow Mach number resp. Laval number covered by the experimental data.

For all cases the outlet flow angle was calculated according to all the "simplified methods" cited above (except [14]), if applicable for variable outlet Mach number, and compared with the experimental data. Three typical examples of the comparison are presented in *FIGURES 28 to 30*.

A case of good agreement for a turbine cascade with rather high deflection shows *fig. 28*. Although the Sine Law value differs by more than 5% the Tangent Law and the Oedegard method coincide nearly perfectly and the Fricke method agrees quite well. Even the decrease and increase of the flow angle with outlet Mach number is very well reproduced. Only the values according to the Jet Deflection Law are far off, as in most cases investigated.

Fig. 29 for a seemingly similar cascade reveals a quite different situation. The Sine Law gives at least a good mean value, the result of the Fricke method is very good, while Tangent Law and Oedegard differ somewhat more. *Fig. 30*, finally, for a quite normal profile form, shows enormous differences in the subsonic range. Especially the variation of outlet flow angle with Mach number is overestimated by all methods dramatically. In the transonic range, however, good agreement exists, which is true for quite a number of cases.

As a resume of the complete investigation it can be stated that no one of the "simplified methods" applied showed a sufficient agreement with experimental results all over the range considered. The differences are differing widely, a correlation with cascade geometry or other relevant parameters could not be found.

6.2 Critical Review of "Simplified Methods"

All the "simplified methods" investigated here are based on the application of the conservation laws for mass flow and momentum in a "control area" limited by the throat of the cascade and a plane with assumed homogeneous flow behind the cascade as shown in *FIGURE 31*. The mass flow and momentum balances are influenced by the conditions along the boundaries of the control area. Only the influences of the rearward stagnation stream lines cancel each other because of the periodicity. The pressure forces in the throat, $K_p a$, on the rearward suction side, $K_p b$, on the trailing edge, $K_p B$, and in the outlet flow plane, $K_p 2$, further the mean velocity vectors in the throat, w_a , and in the outlet flow plane, w_2 , and eventually the friction force, R , on the suction surface enter into the balance equations. Since detailed values for all these quantities are never available for a simplified calculation of the outlet flow angle, the different "simplified methods" apply different assumptions to overcome this inherent problem. These assumptions are described in detail in the pertinent publications cited above; a synopsis is given in [13].

Since the conservation equations for mass flow momentum introduced in the "simplified methods" are inherently correct, any differences between the values calculated by this way and the real values can only be due to the fact, that the mentioned assumptions are not met. A closer examination of this question might reveal the reasons for the experienced deviations and show perhaps means for an improved "simplified method" through a better understanding.

Therefore an extensive study comparing the assumptions of the different "simplified methods" with the real values of the relevant quantities along the boundaries of the control area extracted from numerical flow field calculations and special cascade measurements, as reported above, was conducted and detailed results are reported in [13]. It was found generally, that the constitutive assumptions of the "simplified methods" for calculation of the outlet flow angle are nearly never fulfilled and considerable differences exist. Relatively small modifications in cascade geometry may result in considerable changes of the numerical values of the boundary quantities. Systematic correlations between cascade geometry and the relevant quantities for the balance equations valid for a large range of cascade geometry and operating conditions were not found. This does not exclude the possibility to define such correlations for a small range of geometry variations, i.e. to use "simplified methods" with correction factors or functions for similar "profile families" in a satisfactory and safe way. The necessary corrections, however, have to be determined empirically for each case.

The efforts to correlate the outlet flow angle to specific details of cascade geometry - unsuccessful as they were - led, however, to the formulation of a new general correlation of acceptable accuracy. The ratio of the effective mean outlet flow angle, β_2 , to the outlet flow angle, $\beta_2 \sin \gamma$, calculated according to the Sine Law is correlated to the contraction of the flow channel near the throat expressed as angle γ explained in *FIGURE 32*. The general tendency is well defined, the accuracy is a few percent, based on about 15 cascade configurations.

7. CONCLUSION

Modern numerical methods for the calculation of cascade flow fields render satisfactory results in the compressible-subsonic as well as in the transonic region, as long as boundary layer separation does not occur. For comparison with experimental data the use of the actual and accurate cascade geometry and the experimental value of the axial velocity density ratio in the calculation is indispensable.

With appropriate treatment of the trailing edge - even with considerable thickness - either by introduction of suitable wake flow models or assumptions into the computer code or by competent judgement of the results and controlled adaption of the input data, these calculating methods will render values for the outlet flow angle with an accuracy sufficient for industrial demands, i.e. of a few tenth of a degree.

"Simplified methods" for the calculation of the outlet flow angle, based on mass flow and momentum balance with generalized assumptions for the outlet area of a cascade only, are not capable to take sufficiently into account the real flow field and the specific nature of the boundary conditions and will hardly ever achieve the necessary accuracy. Application of these methods is only advisable within narrow ranges of cascade geometry and with empirically determined corrections or adaptations.

References

- [1] Heinemann, H.-J. The Test-Facility for Rectilinear Cascades (EGG) of the DFVLR
DFVLR Bericht IB 222 - 83 A 14 (1983)
- [2] Lehthaus, F. Berechnung der transsonischen Strömung durch ebene Turbinengitter nach dem Zeitschrittverfahren
VDI-Forschungsheft 686, S. 5-24
VDI-Verlag, Düsseldorf (1978)
- [3] Kiock, R. The Transonic Flow Through a Plane Turbine Cascade as Measured in Four European Wind Tunnels
Lehthaus, F. ASME Journal of Engineering for Gas Turbines and Power, Vol. 108, p. 285-292, (1986)
Baines, N.
Sieverding, C.
- [4] Amecke, J. Anwendung der transsonischen Ähnlichkeitsregel auf die Strömung durch ebene Schaufelgitter
VDI-Forschungsheft 540, S. 16-28
VDI-Verlag, Düsseldorf (1970)
- [5] Giess, P.-A. Theoretische Untersuchungen mit Hilfe eines 2-d-Zeitschrittverfahrens an drei Turbinengittern
DFVLR Bericht IB 222 - 85 A 35 (1986)
- [6] Katsanis, Th. Computer program for Calculating Velocities and Streamlines on a Blade-to-Blade Stream Surface of a Turbomachine
NASA TN D - 4525 (1968)

- [7] Dalbert, P. Untersuchung der Strömung und der Verluste an Turbinenschaufelgittern zur Bestimmung des Abströmwinkels
Abschlußbericht zum FVV-Forschungsvorhaben
"Abströmwinkel II"
FVV-Heft Nr. 368 (1985)
- [8] Bammert, K. Der Einfluß verdickter und verdünnter Turbinenschaufeln
Sonnenschein, H. auf die Gittereigenschaften
Archiv für das Eisenhüttenwesen 38 (1967),
Nr. 4, S. 287
- [9] Traupel, W. Prediction of Flow Outlet Angle in Blade Rows with
Conical Stream Surfaces
ASME Paper 73-GT-32 (1973)
- [10] Fricke, H. Beitrag zur Ermittlung des Abströmvektors aus Turbinen-
gittern für den unter- und überkritischen Bereich
VDI-Bericht Nr. 264 (1976), S. 25 pp.
- [11] Oedegard, S. Der Abströmwinkel von Turbinenleitschaufeln als Funktion
der Machzahl und der Teilung
Mitt. Inst. f. Strahlantriebe und Turboarbeitsma-
schinen, RWTH Aachen, Nr. 74-04 (1974)
- [12] Traupel, W. Die Strahlablenkung in der vollbeaufschlagten Turbine
Mitt. Inst. Therm. Turbomaschinen, ETH Zürich,
Nr. 3 (1956), S. 27 pp.
- [13] Dalbert, P. Der Abströmwinkel von Turbinen-Schaufelgittern,
Leistungsfähigkeit und Grenzen von Berechnungsverfahren
Dissertation, Universität Hannover (1986)
- [14] Bräunling, W. Prediction of Flow Outlet Angle in Rotating Annular Turbine
Cascades with Conical Stream Surfaces in Subsonic and
Transonic Flow Regimes
Thermische Strömungsmaschinen '85, Bochum 17/18. Sept. 1985
VDI Verlag, Düsseldorf (1985)

Acknowledgments

The investigations have been initiated by Forschungsvereinigung Verbrennungskraftmaschinen e.V. (FVV), Frankfurt/Main, and have been sponsored by Ministry of Economics via Arbeitsgemeinschaft Industrieller Forschungsvereinigungen e.V. (AIF), Köln. The authors wish to thank Mr. H. Bals, Kraftwerk-Union/Mülheim, chairman of the FVV working group, and Dr. F. Lehthaus, DFVLR/Göttingen, head of the cascade group, for intensive discussions when performing the FVV contract.

cascade	β_s	t/l	β_1	c^*/t	d/t
3.1.1	49.0°	0.680	94.0°	0.4489	0.0115
10.1.2	70.0°	0.600	130.0°	0.5458	0.0159
10.1.2I	70.0°	0.600	130.0°	0.5458	-
10.SSV1	70.0°	0.586	130.0°	0.5460	0.0789
10.SSV2	70.0°	0.593	130.0°	0.5460	0.0473
17.1.1	71.0°	0.499	118.0°	0.4246	0.0673

TABLE 1: Geometrical values of the investigated cascades

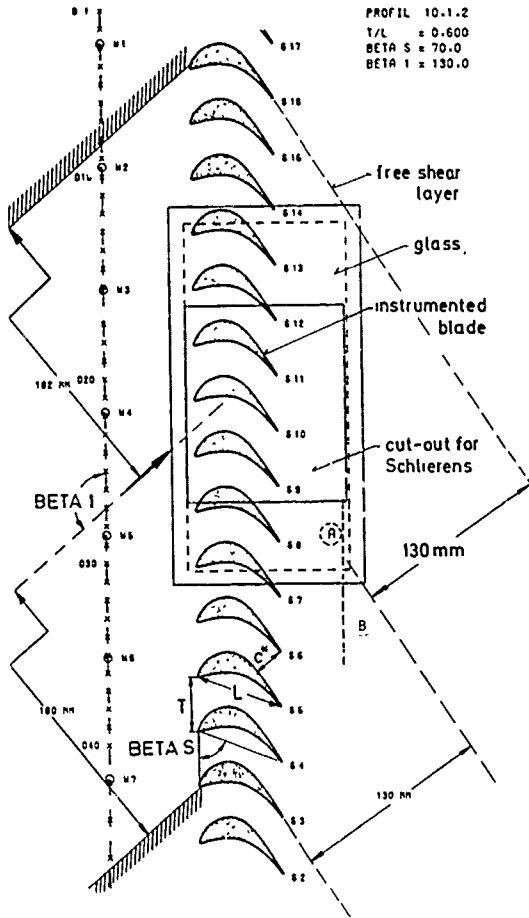


FIGURE 1: Test set-up

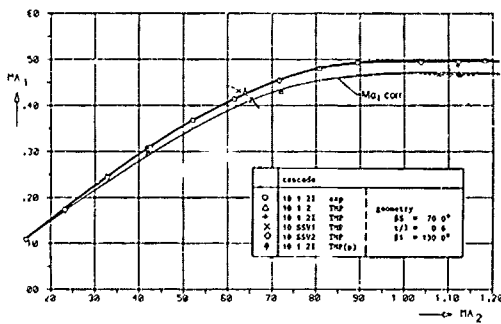


FIGURE 3: Upstream Mach number of homogeneous flow

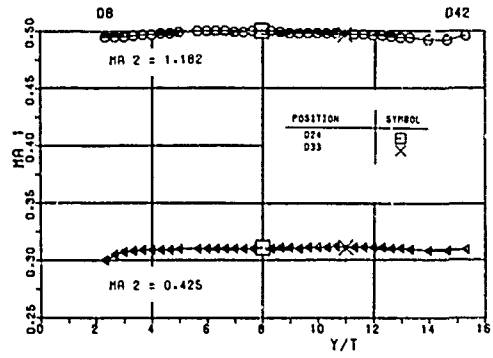


FIGURE 2: Inlet Mach number distribution versus inlet nozzle height

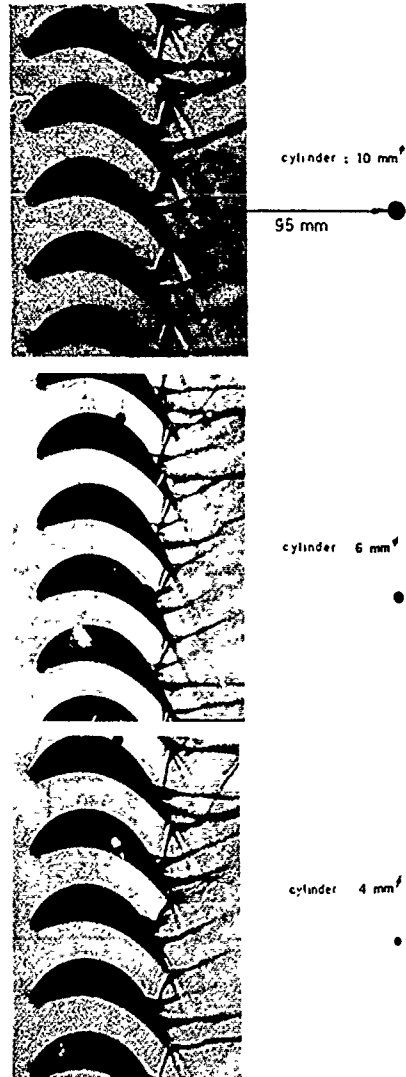


FIGURE 4: Cylinders in a downstream supersonic cascade flow ($Ma_2 \approx 1.2$)

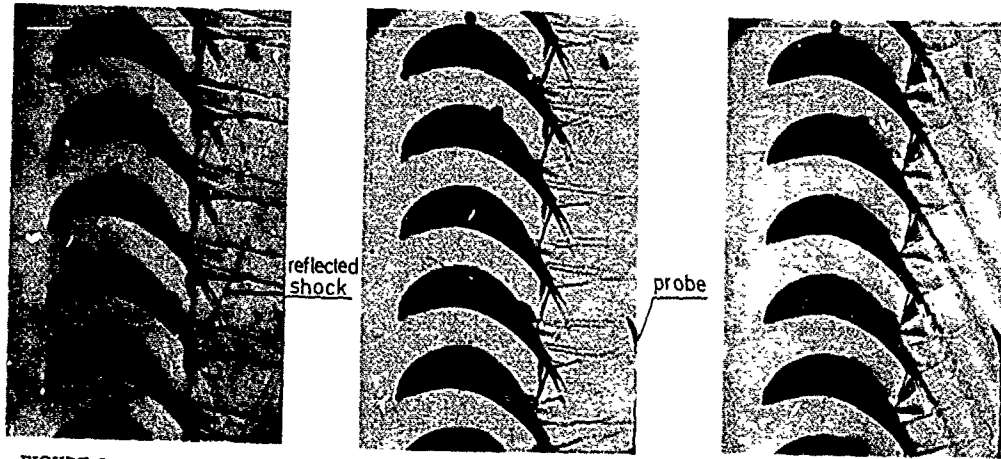


FIGURE 5: Wedge-probe, supported with the new probe-holder

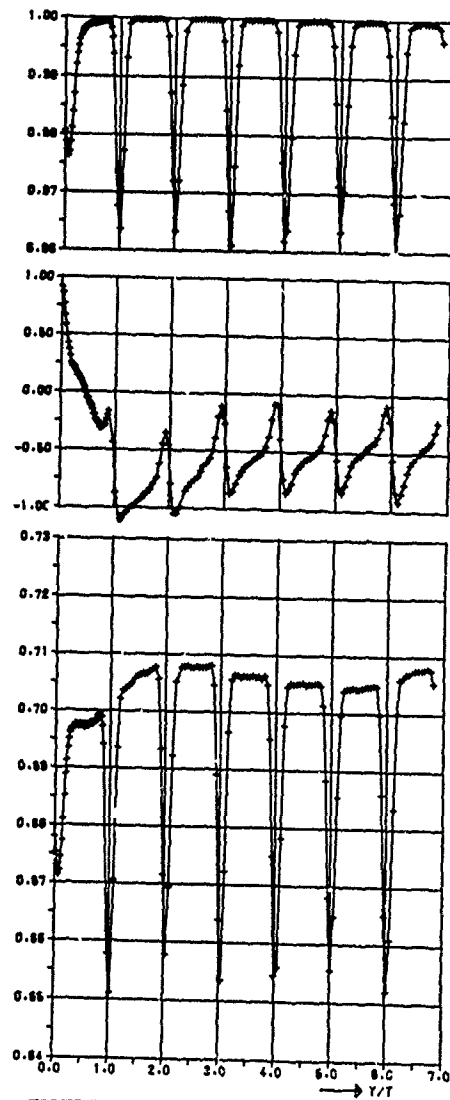


FIGURE 6: Local flow quantities (subsonic)

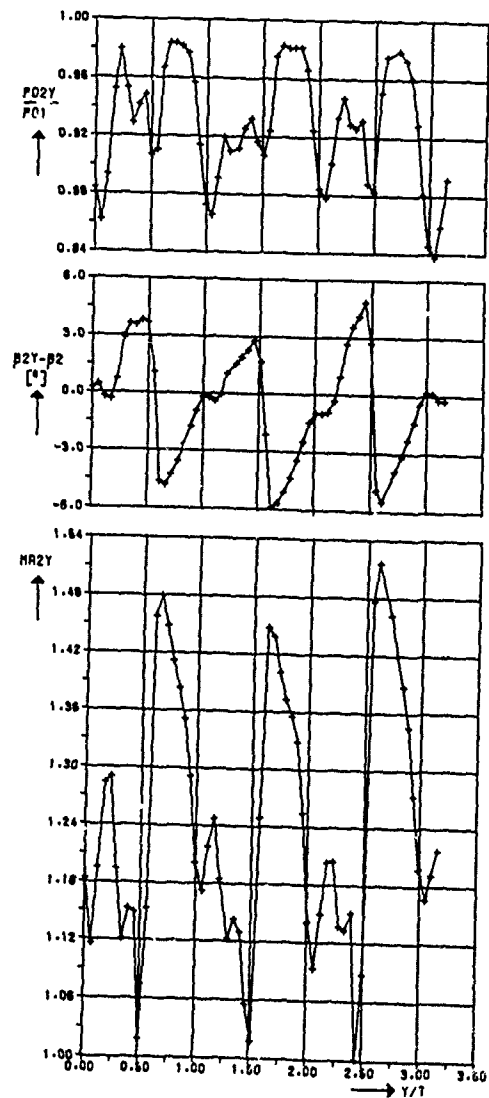


FIGURE 7: Local flow quantities (supersonic)

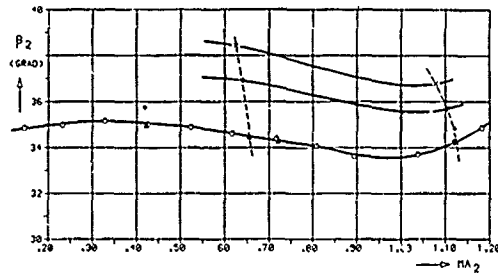


FIGURE 8: Downstream flow angle of homogeneous flow

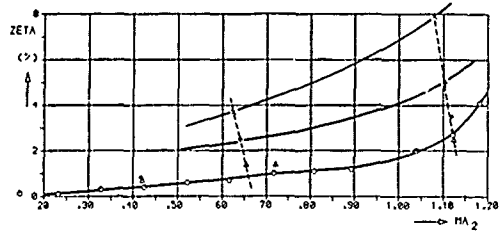


FIGURE 9: Total pressure loss coefficient of homogeneous flow

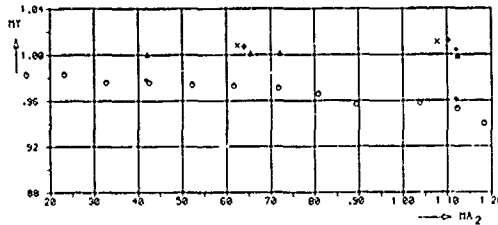


FIGURE 10: Axial velocity density ratio of homogeneous flow

cascade		
○	10.1.21	exp
△	10.1.2	TMP
+	10.1.21	TMP
x	10.SSV1	TMP
◇	10.SSV2	TMP
◆	10.1.21	TMP(u)
		geometry
		SS = 70.0°
		t/l = 0.6
		δ1 = 130.0°

Symbols used in fig. 8, 9 and 10

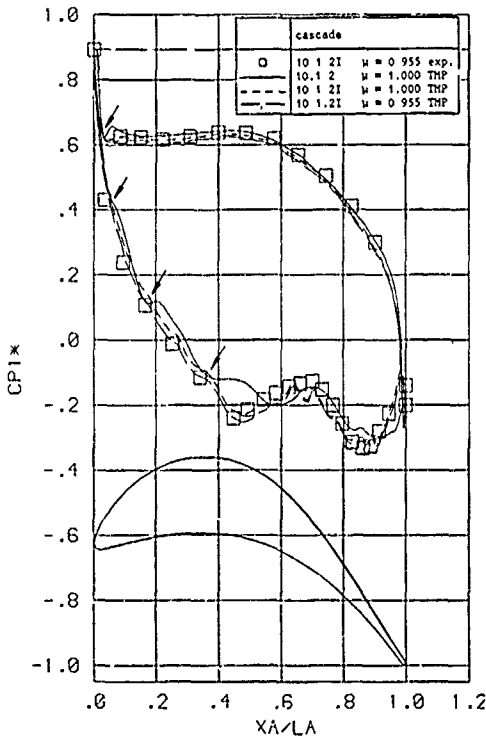


FIGURE 11: Surface pressure distribution (Ma_{2is} = 1.144)

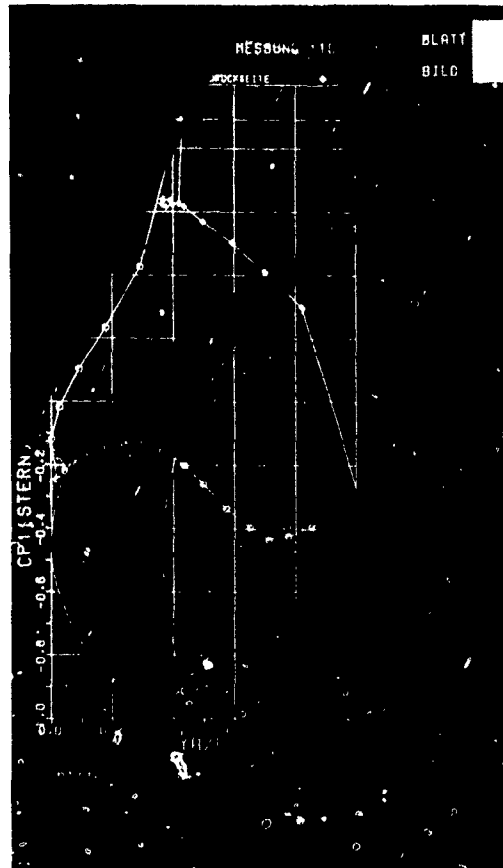


FIGURE 12: Surface pressure distribution with Schlieren picture

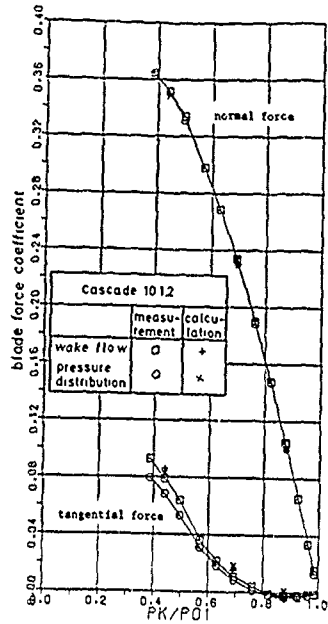


FIGURE 13: Blade force coefficients

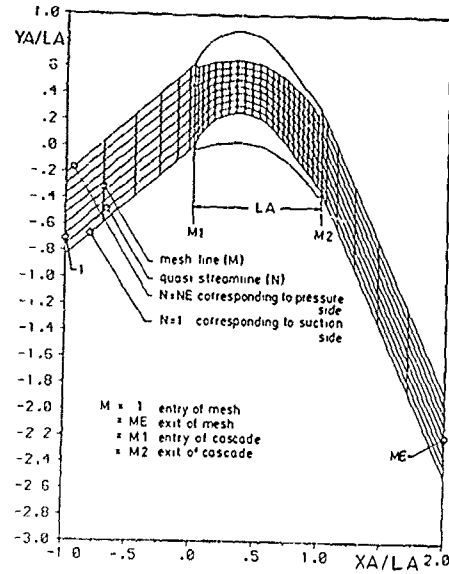


FIGURE 14: Definitions within the computational mesh

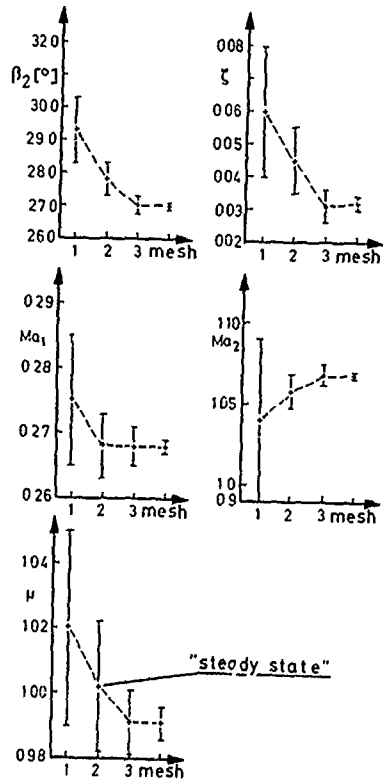


FIGURE 15: Maximum deviation from the steady state solution after 10, 20, 40 and 80 time intervals corresponding to the four meshes

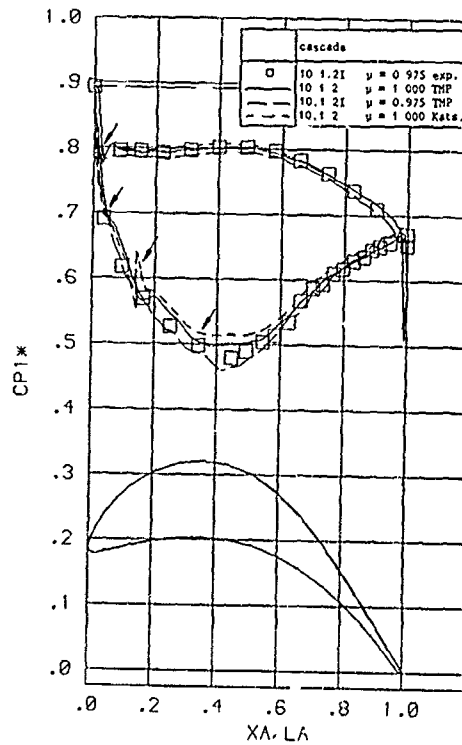


FIGURE 16: Surface pressure distribution (Ma2is = 0.433)

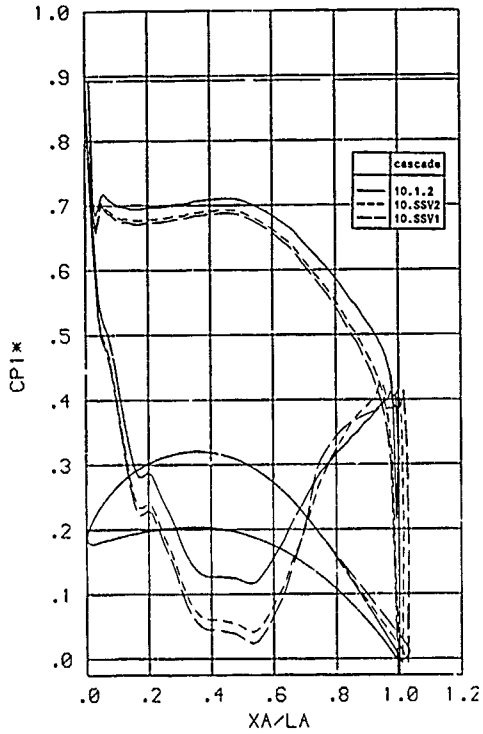


FIGURE 17: Surface pressure distribution (Ma_{2is} = 0.670)

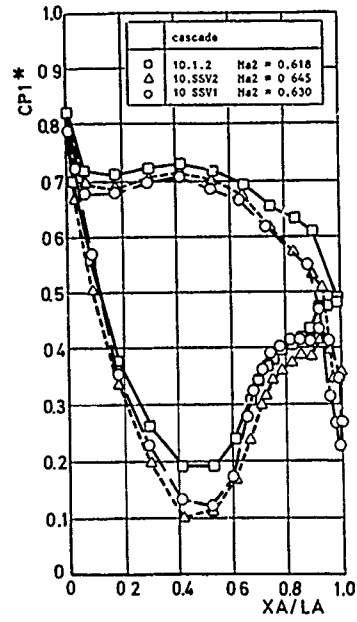


FIGURE 18: Surface pressure distribution from experiments

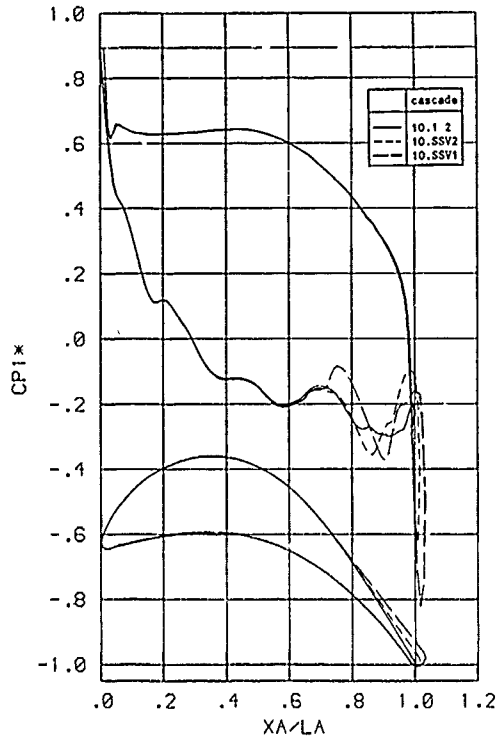


FIGURE 19: Surface pressure distribution (Ma_{2is} = 1.144)

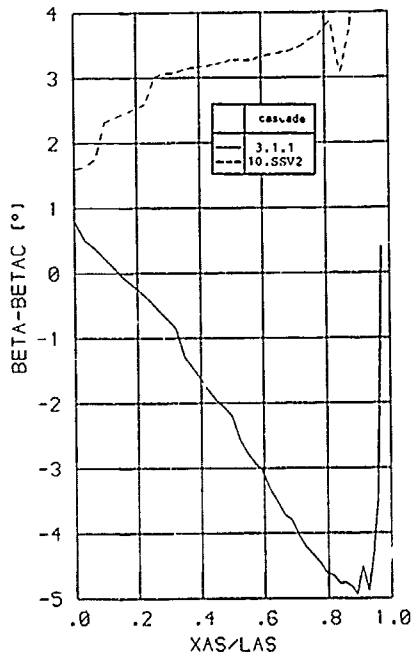


FIGURE 20: Deviation of the local flow direction from perpendicular flow through the throat

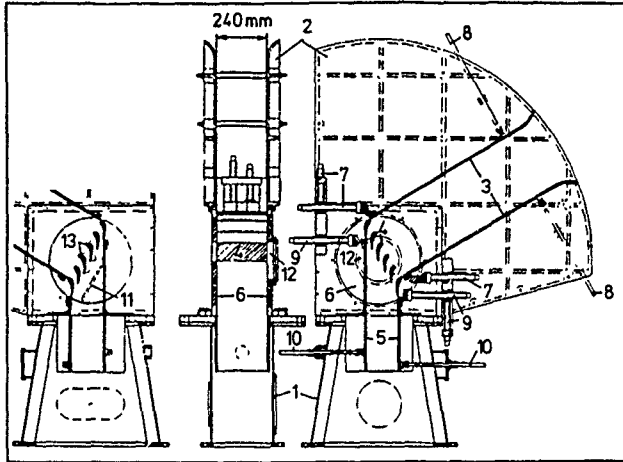


Fig. 21
Suction-type Cascade
Wind Tunnel (IFS Hannover)

- 1 - Outlet Plenum
- 2 - Side Walls
- 3 - Inlet Guide Plates
- 4 - Cascade
- 5 - Outlet Guide Plates
- 6 - Cascade Holding Plate
- 7, 8, 9, 10 - Adjusting Screws
- 11 - Probe Slot
- 12 - Window
- 13 - Pressure Meas. Profiles

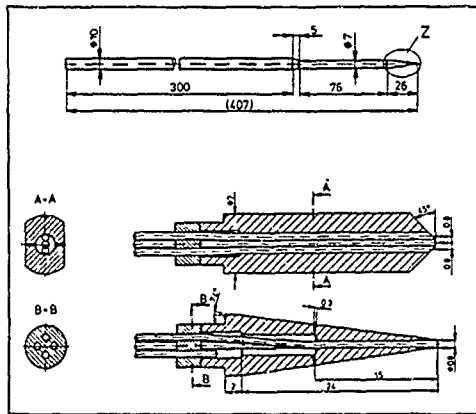


Fig. 22 Wedge-Type Five Hole Probe

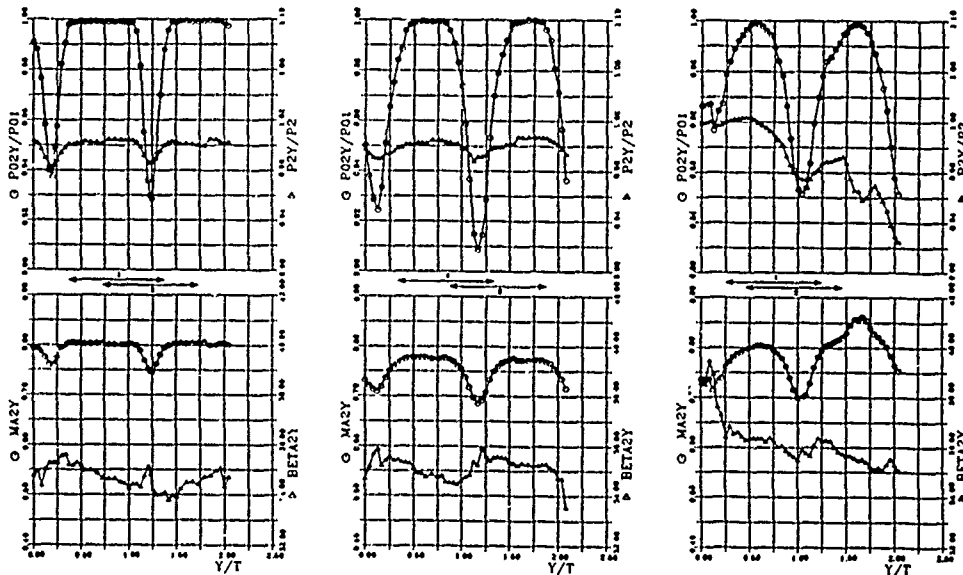


Fig. 23 Downstream Flow of Cascade 10.1.2 with Ratio of Trailing Edge to Pitch 0,016; 0,04; 0,075

PO2 - Total Pressure MA2 - Outlet Mach Nb.
 P2 - Static Pressure BETA2 - Outlet Angle

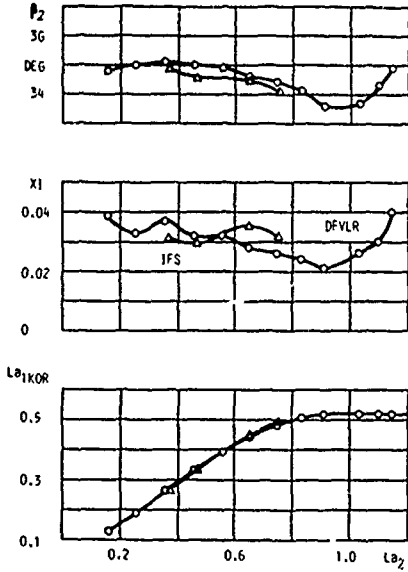


Fig. 24 Comparison of Test Results of Cascade 10.1.2

- La₂ - Outlet Laval Nb.
- XI - Loss Coefficient
- β₂ - Outlet Angle
- La₁ - Inlet Laval Nb. (corrected)

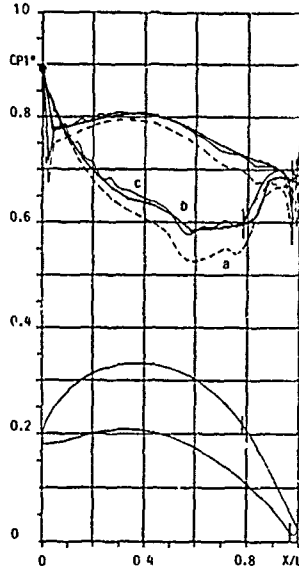


Fig. 25 Comparison of Measured and Calculated Pressure Distribution for Cascade 17.1.1

- a - Katsanis-Calculatoin
- b - Katsanis-Calc. with Correction
- c - Experimental

$$La^2 = Ma^2 \cdot \frac{Ma^2}{1 + \frac{\gamma - 1}{\gamma + 1} (Ma^2 - 1)}$$

for ideal gases with constant specific heat

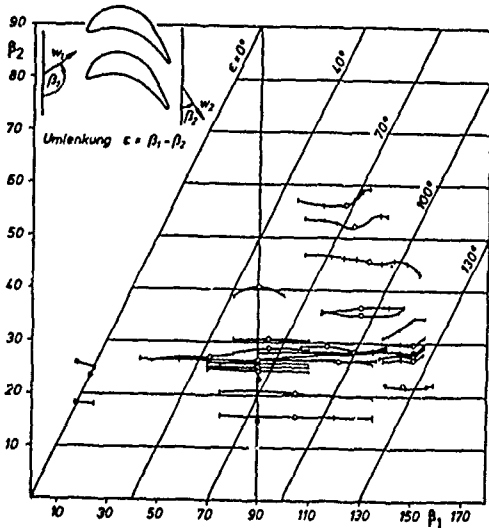


Fig. 26 Flow Angle Characteristics of Investigated Cascades

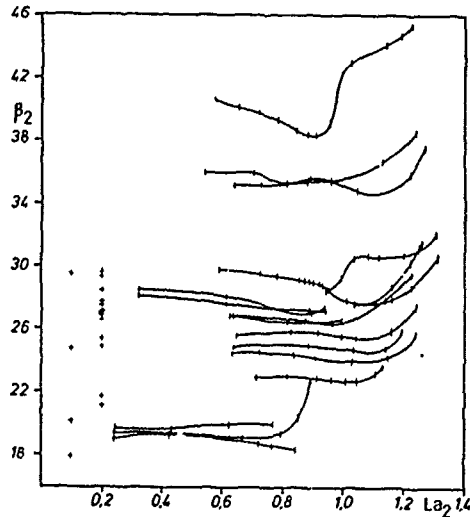


Fig. 27 Laval Number Range of Investigated Cascades

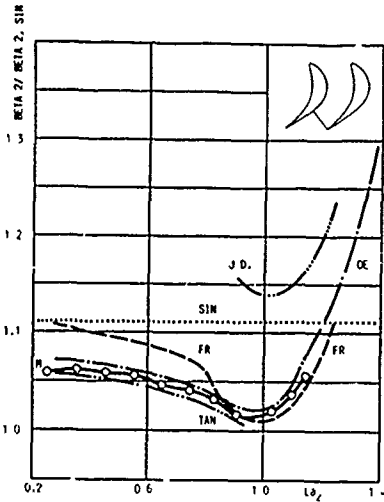


Fig. 28
Outlet Flow Angle vs. Outlet Laval Number for Cascade 10.1.2, Comparison of Measurement with Simplified Calculations

SIN - Sine Law OE - Oedegard
TAN - Tangent Law FR - Fricke
J.D. - Jet Deflection M - Measurements (DFVLR)

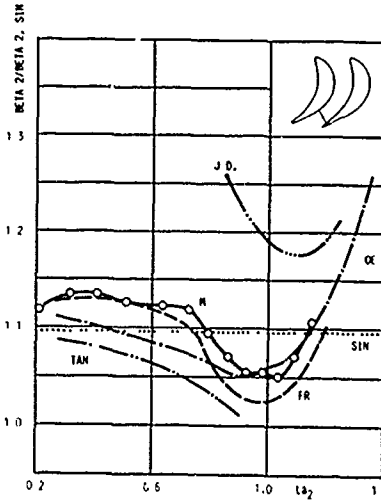


Fig. 29 Outlet Flow Angle vs. Outlet Laval Number for Cascade 17.1.1 (see Fig. 28)

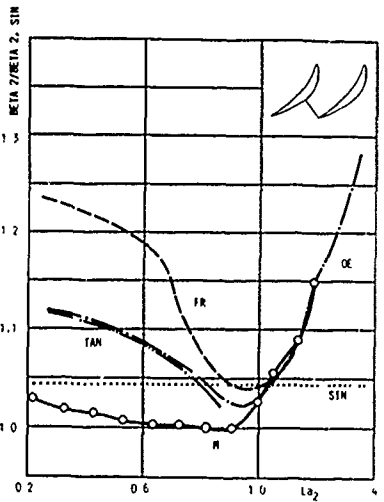


Fig. 30 Outlet Flow Angle vs. Outlet Laval Number for Cascade 3.1.1 (see Fig. 28)

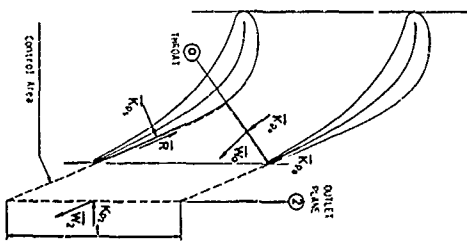


Fig. 31 Control Area for "Simplified Methods" with Relevant Parameters

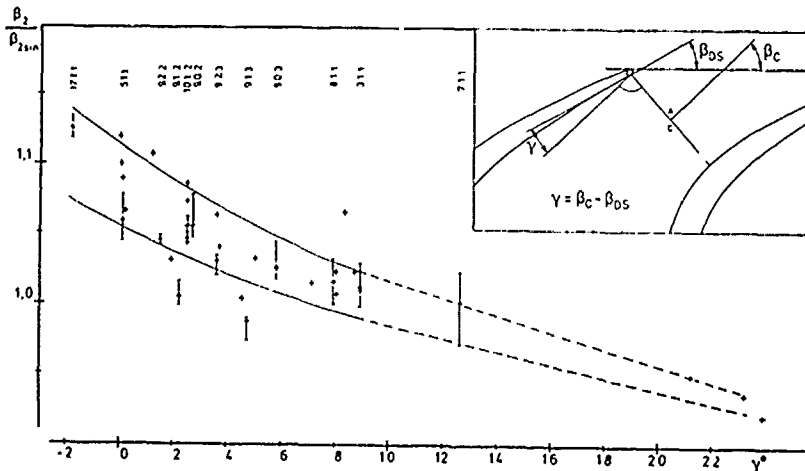


Fig. 32
Outlet Flow Angle Correlation vs. Contraction Angle of Flow Channel

DISCUSSION

H.A.Schreiber, Ge

We know that the AVDR can have a strong influence on the downstream flow angle. Have you considered the AVDR influence in the β correlation?

Author's Reply

The correlation presented in Figure 32 is at present purely empirical and no corrections are included. The correction proposed is surely possible, but we did not work on this further refinement of the correlation, because we are not convinced of the general applicability of any correlation based only on simple geometric parameters.

J.D.Denton, UK

In Figures 28, 29, 30 why is the value of $\beta_2/\sin \beta_2$ equal to 1 for the sine rule?

Did you make any comparisons of the outlet angle predictions from the computational methods with the measurements?

If not I think that it would be a very useful exercise.

Author's Reply

$\beta_2 \sin \beta_2$ is taken from the simple sine law

$$\beta_2 \sin \beta_2 = \arcsin a/t$$

a = throat width

t = pitch

SIN in the diagrams is the result of a corrected sine law as presented f.t. in Reference 8 or in Traupel: Termische Turbomaschine, which takes into account the trailing edge thickness.

The downstream flow angles calculated by the time-marching code compare in general well with experimental data, see Figure 8 of the paper. The subsonic Katsanis code demands actually to specify the downstream angle. An iterative calculation based on visual judgement of the pressure distribution calculated around the trailing edge normally gives results accurate to a few tenths of a degree. Introduction of a suitable outflow condition into the Katsanis code seems well possible as described in the paper.

